This article has been accepted for publication in a future issue of this journal, but has not been fully edited. Content may change prior to final publication. Citation information: DOI 10.1109/TPEL.2018.2849104, IEEE Transactions on Power Electronics

Low-Capacitance StatCom with Modular Inductive Filter

Glen Farivar, *Member, IEEE*, Christopher Townsend, *Member, IEEE*, Josep Pou, *Fellow IEEE*, Branislav Hredzak, *Senior Member, IEEE*

Abstract

In this paper, a cascaded H-bridge low-capacitance StatCom (LC-StatCom) with a modular inductive filter is introduced. Replacing the fixed-value filter inductors with tyristor switched reactors, a well-developed member of the static VAr compensators family, reduces the overall energy storage capacity and voltage rating of the LC-StatCom without violating standard limits on current quality. The proposed modular inductive filter takes advantage of LC-StatCom's ability to synthesize high quality ac voltage to reduce the overall energy storage requirement of the filter inductance. The proposed modular filter inductor concept adds an additional degree of freedom to control the maximum voltage drop on the filter inductor by changing the inductance value. This additional capability decreases the overall voltage rating of the converter. The effects of adding the modular inductor unit on the I-V characteristic of the LC-StatCom are evaluated. The effectiveness of the proposed solution is demonstrated by experimental results on a 7-level 0.7 kVA LC-StatCom.

***Index Terms*— Cascaded H-bridge, LC-StatCom, modular inductor, reactive power compensation**

This manuscript was submitted for review November 12, 2017; revised February 12, 2018 and May 08, 2018; accepted Jun 09, 2018. This paper has not been published or submitted for publication in any other conference or journal article.

Glen Farivar is with the Nanyang Technological University, Energy Research Institute (ERI@N), Singapore 637141, e-mail: gfarivar@ntu.edu.sg.

Christopher Townsend is with the Nanyang Technological University, School of Electrical and Electronics Engineering, Singapore 639798, e-mail: townsend@ieee.org.

Josep Pou is with the Nanyang Technological University, School of Electrical and Electronics Engineering, Singapore 639798, e-mail: j.pou@ntu.edu.sg.

Branislav Hredzak is with the University of New South Wales (UNSW Australia), School of Electrical Engineering and Telecommunication, Sydney, NSW 2052 Australia, e-mail: b.hredzak@unsw.edu.au.

Corresponding author: Glen Farivar, Email: gfarivar@ntu.edu.sg, Phone: +65 84339635, Fax: +65 66946217, Address: 1 Cleantech Loop, #02-24, Singapore 637141.

This article has been accepted for publication in a future issue of this journal, but has not been fully edited. Content may change prior to final publication. Citation information: DOI 10.1109/TPEL.2018.2849104, IEEE Transactions on Power Electronics

I. INTRODUCTION

The requirement of multiple isolated dc sources is an important disadvantage of cascaded H-bridge (CHB) multilevel converters. However, in applications such as StatComs, where isolated dc sources are readily available as capacitors, this drawback is eliminated. A CHB StatCom is a well-established and commercially available technology, where many of its aspects and applications was explored and developed in the literature [1-19]. Recent advancements in CHB StatCom technology covers a wide range of aspects including, fault tolerance and unbalanced load operation [20-24], voltage and current control [22-27], modulation based on model predictive control [28-30], PWM switching and its effect [20], [31], [32], and decentralized control design [33].

A CHB converter is essentially based on single-phase units. In other words, a three-phase CHB StatCom is merely composed of three single-phase units. Therefore, large capacitor banks are necessary to buffer the sinusoidal power oscillations. The dc capacitor size is traditionally designed to limit the ripple on the capacitor voltage to less than 10% of nominal dc voltage [19].However, reducing the cost, weight, and volume along with improving reliability of the system are among major motives to reduce the size of dc capacitors as much as possible.

Reducing capacitor size means increasing ripple on the capacitor voltages. This leads to unacceptable maximum dc voltage levels [17]. One way to limit the maximum voltage while increasing ripple on capacitor voltages is to use phase alignment of the inverter's ac side voltage and the capacitor voltage ripple [34-40]. This alignment, utilized in a so called low-capacitance StatCom (LC-StatCom), only occurs in the capacitive region.

LC-StatCom is suited for film capacitors due to the required low capacitance values and large voltage ripple. Due to the use of film capacitors, reliability of the LC-StatCom is expected to be higher than the conventional StatCom with electrolytic capacitors [41], [42]. Lower average dc capacitor voltage also results in lower switching losses, which translates into improved efficiency [40]. In [34], the operational principal and different operation modes of StatCom with reduced capacitor size are outlined. [37] and [38] focused on improving the controller dynamics to regulate the peak capacitor voltage. In [34], the operational limit of the LC-StatCom is calculated. LC-StatCom by nature is not suitable to operate in the inductive mode, which is considered to be its main drawback. This drawback was addressed in [39], where an additional thyristor bypassed reactor (TBR) was used in series with the filter inductor to provide symmetrical capacitive and inductive reactive power generation capacity. Overall, the LC-StatCom technology is still under development and many aspects of it remain unexplored.

This article has been accepted for publication in a future issue of this journal, but has not been fully edited. Content may change prior to final publication. Citation information: DOI 10.1109/TPEL.2018.2849104, IEEE Transactions on Power Electronics

As demonstrated in [35], LC-StatCom uses the ripple on the capacitor voltage to generate higher quality ac voltages. To elaborate further, in LC-StatCom, the alignment of the ac output voltage and capacitor voltage ripple maintains a high number of levels in the output voltage, even during parts of the fundamental period when the value of the synthesized output voltage is low. To keep harmonic performance similar to that of the conventional StatCom, the superior waveform quality of the LC-StatCom could facilitate the use of a smaller filter inductor when operating close to nominal rms StatCom current. However, when the rms StatCom current is low, the capacitor voltage ripple decreases and its positive effect on voltage total harmonic distortion (THD) diminishes, which leads to increased current total demand distortion (TDD). Therefore, LC-StatCom is unable to utilize its superior voltage quality and the filter inductance remains comparable to a conventional StatCom. However, if the voltage drop across this inductor is reduced then this lowers the voltage rating of the LC-StatCom, which will make the LC-StatCom cheaper, smaller, and lighter.

In this paper, a modular variable filter inductor is proposed as a solution to achieve the mentioned benefits of low filter inductance. Using the proposed modular inductor concept, the inductance increases as the current decreases to compensate for the adverse effect of reduced capacitor voltage ripple on the current TDD. The overall energy storage capacity of the proposed filter inductor remains significantly smaller than a fixed inductor, while maintaining current TDD lower than the allowed limit.

The structure of this paper is as follows. A brief introduction of LC-StatCom system is provided in Section II. The effect of capacitor voltage ripple on the LC-StatCom's ac-side voltage quality is examined in Section III. The proposed modular inductive filter concept is introduced in Section IV. Some additional comments for designing modular filter inductor are provided in Section V. Simulations and control circuits are provided in Section VI. Experimental results are given in Section VII. Finally, the main conclusions of this work are summarized in Section VIII.

II. CASCADED H-BRIDGE LC-STATCOM

LC-StatCom's operational principle is based on the premise of keeping the instantaneous capacitor voltage higher than the absolute value of the grid voltage. In the capacitive region, the main component of the capacitor voltage ripple and the absolute value of the grid voltage have an equal phase angle (neglecting losses). This allows

This article has been accepted for publication in a future issue of this journal, but has not been fully edited. Content may change prior to final publication. Citation information: DOI 10.1109/TPEL.2018.2849104, IEEE Transactions on Power Electronics

for the ripple on the capacitors to grow without increasing the maximum capacitor voltage or going below the grid voltage. This concept is shown in Fig. 1.

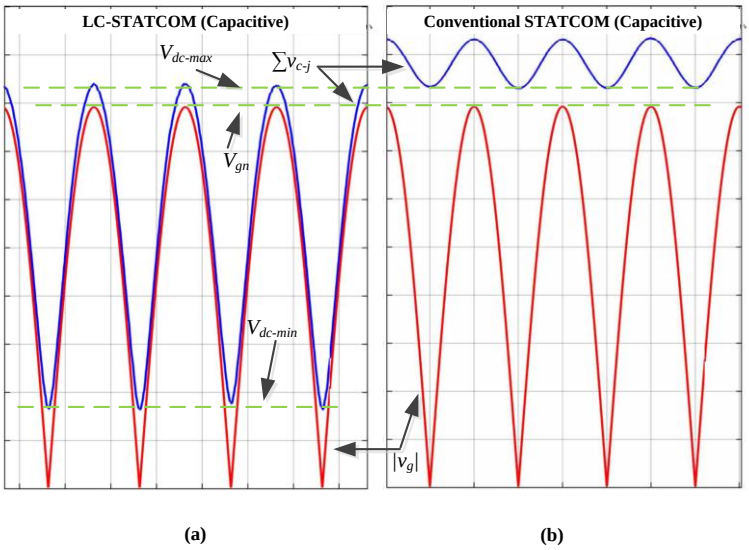

Fig. 1. Operation principal of LC-StatCom.

The operational limits of an ideal LC-StatCom (neglecting the losses and filter inductor) are as follows [34]

Capacitive:

$$0 \le I_{q(p.u)} \le 1 \quad , \quad (0 \le V_{g(p.u)} \le 1). \tag{1}$$

Inductive:

$$\begin{aligned} 0 < I_{q(p.u)} &\le \frac{1}{V_{g(p.u)}} - V_{g(p.u)} \quad , \quad (0.62 \le V_{g(p.u)} \le 1) \\ 0 < I_{q(p.u)} &\le 1 \qquad\qquad\qquad , \quad (0 \le V_{g(p.u)} < 0.62) \end{aligned}. \tag{2}$$

$I_{q(p.u)}$ and $V_{g(p.u)}$ are the per unit values of reactive current and grid voltage, respectively. The operational limits defined in (1) and (2) are shown graphically in Fig. 2. As the figure suggests, LC-StatCom is mainly suitable to operate in capacitive mode. LC-StatCom with a symmetrical I-V characteristic requires adding a TBR unit [39]. Therefore, for the rest of this paper only capacitive operating mode is assumed.

This article has been accepted for publication in a future issue of this journal, but has not been fully edited. Content may change prior to final publication. Citation information: DOI 10.1109/TPEL.2018.2849104, IEEE Transactions on Power Electronics

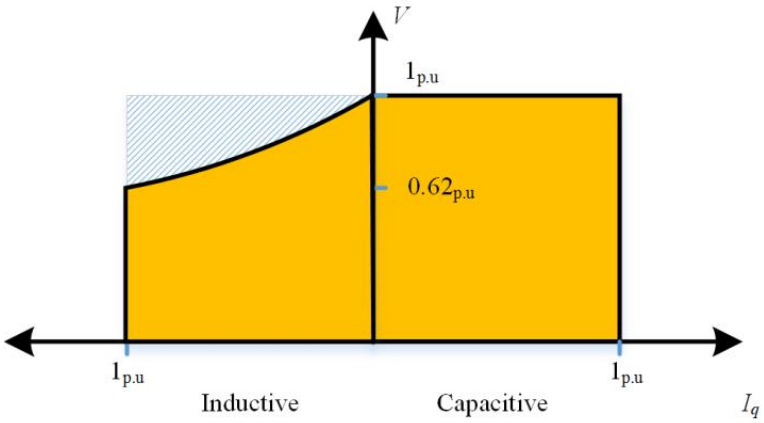

Fig. 2. I-V characteristics of an ideal LC-StatCom.

The reference signal for the cluster capacitor voltage controller, $V^2_{0\text{-}ref}$, in LC-StatCom is a function of current in order to keep the maximum capacitor voltage constant [34], as follows:

$$V_{0-ref}^2 = \frac{V_{dc-max}^2}{N} - \frac{V_g + X_L I_{q-ref}}{4\pi f_g C} I_{q-ref} \tag{3}$$

In (3), X_L is the reactance of the ac side filter inductor and $I_{q\text{-}ref}$ is the reactive current reference of the LC-StatCom. N is the number of H-bridge modules, f_g is the grid frequency, V_g is the grid voltage magnitude, and C is the capacitance of dc side capacitors (capacitance per cell). The LC-StatCom control system can keep $V_{dc\text{-}max}$ fixed for all values of $I_{q\text{-}ref}$ within its operational limits. These limits in capacitive and inductive regions are not symmetrical. At full capacitive load, the minimum instantaneous value of the cluster voltage hits its minimum allowed value, $V_{dc\text{-}min}$. The nominal reactive power, I_{qn}, is calculated as

$$I_{qn} = \frac{V_{dc-\max}^2 - V_{dc-\min}^2}{V_{gn} N} \frac{2\pi f_g C}{1 + X_{L(p.u)}}, \tag{4}$$

in which, $X_{L(p.u)}$ represents the per-unit value of the filter inductor and V_{gn} is the nominal grid voltage magnitude.

This article has been accepted for publication in a future issue of this journal, but has not been fully edited. Content may change prior to final publication. Citation information: DOI 10.1109/TPEL.2018.2849104, IEEE Transactions on Power Electronics

III. Effect of Capacitor Voltage Ripple on Quality of Generated AC Voltage

Unlike the conventional CHB StatCom, in which the ripple on the capacitors is considered a disturbance, the LC-StatCom benefits from it to improve its synthesized ac voltage profile. In this section, the effect of the capacitor voltage ripple on the quality of synthesized ac voltage of a H-bridge converter is investigated. Ignoring the effect of switching harmonics, the capacitor voltage, v_C, is

$$v_C(t) = \sqrt{V_{C-\max}^2 + \frac{I_g V}{4\pi f_g C}(\sin(4\pi f_g t) - 1)}. \tag{5}$$

In (5), I_g is the peak value of the grid current and V is the peak value of the ac side voltage, v.

In capacitive mode, LC-StatCom can operate with theoretical 100% ripple on the capacitor voltage. The resulting THD of the pulse width modulated ac voltage waveform is defined as

$$THD = \frac{\sqrt{\sum_{n\neq 1} V_{pwm}^2(n)}}{V_{pwm}(1)} \tag{6}$$

where, $V_{pwm}(n)$ represents the RMS value of nth order harmonic of the pulse-width modulated ac voltage, v_{pwm}. $\sqrt{2}V_{pwm}(1)$ is the magnitude of the desired sinusoidal ac voltage, V. Note that THD in (6) is independent of the switching frequency and varies with V and the rms value of capacitor voltage, $V_{C\text{-}rms}$ as follows:

$$THD = \frac{\sqrt{2V_{C-rms}^2 - V^2}}{V}. \tag{7}$$

The THD as a function of the reactive current, I_g, can be easily derived by calculating $V_{C\text{-}rms}$ from (5) and replacing it in (7), as follows:

This article has been accepted for publication in a future issue of this journal, but has not been fully edited. Content may change prior to final publication. Citation information: DOI 10.1109/TPEL.2018.2849104, IEEE Transactions on Power Electronics

$$THD = \frac{\sqrt{2V_{C-\max}^2 - I_g V/(2\pi f_g C) - V^2}}{V}. \tag{8}$$

Rewriting (8) in per-unit form yields,

$$THD = \frac{\sqrt{2 - I_{g(p.u)} V_{(p.u)} - V_{(p.u)}^2}}{V_{(p.u)}}. \tag{9}$$

In (9), $V_{C\text{-}max}$ is the base value of the voltages and $2\pi f_g C V_{C\text{-}max}$ is the base value for the current. Therefore, at nominal (1 per-unit) operating condition, the capacitor voltage reaches zero at its minimum.

Increasing V and I_g increases the capacitor voltage ripple and consequently reduces the THD. The capacitor voltage ripple, r, is defined as:

$$r = 1 - v_{C-\min(p.u)}. \tag{10}$$

In (10), $v_{C\text{-}min(p.u)}$ represents normalized minimum capacitor voltage (using $V_{C\text{-}max}$ as the base voltage). THD variation as a function of r can be easily derived by: First substituting $v_{C\text{-}min(p.u)}$ from (5) to derive the expression of $I_{g(p.u)}V_{(p.u)}$ in terms of r:

$$I_{g(p.u)} V_{(p.u)} = 1 - (1-r)^2. \tag{11}$$

Then, from (9) and (11), the THD can be rewritten as

$$THD = \frac{\sqrt{1 + (1-r)^2 - V_{(p.u)}^2}}{V_{(p.u)}}. \tag{12}$$

In practice, $V_{(p.u)}$ does not change in a wide range and remains close to one per-unit. Therefore, for the theoretical ideal case of $V_{(p.u)}$=1, (12) can be simplified as

$$THD = 1 - r. \tag{13}$$

This article has been accepted for publication in a future issue of this journal, but has not been fully edited. Content may change prior to final publication. Citation information: DOI 10.1109/TPEL.2018.2849104, IEEE Transactions on Power Electronics

Equation (13) shows that the voltage THD in LC-StatCom varies linearly with the ripple magnitude. Hence, the ac side voltage of an LC-StatCom designed to operate with r=0.5 at rated condition will have approximately half the THD compared to a conventional StatCom with $r\approx0$. The PWM output voltage for both of these cases is shown in Fig. 3. This figure is obtained using an ideal triangular two-level PWM generator with carrier frequency of 41 times the reference voltage frequency. In Fig. 3(b) the dc voltage profile is generated by an ideal controllable voltage source, which varies according to (5).

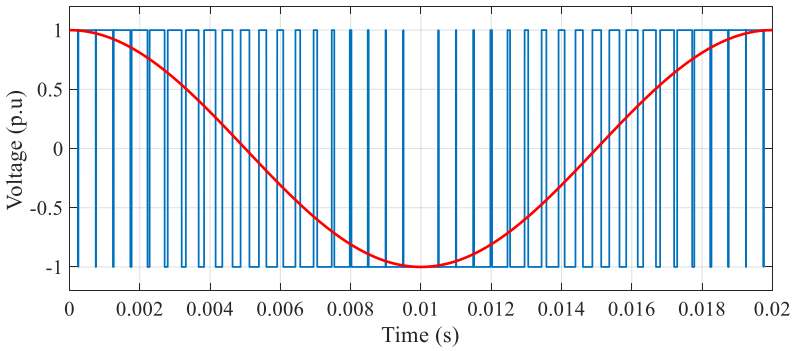

(a)

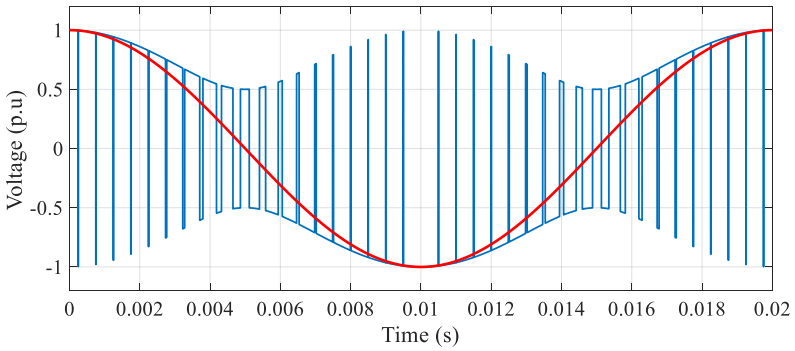

(b)

Fig. 3. Synthesized PWM ac voltage for (a) $r\approx0$ and (b) r=0.5.

As it can be observed in Fig. 3(b), the sinusoidal shape of the capacitor voltage ripple helps the instantaneous modulation index to remain high throughout the fundamental period, which results in a better utilization of the capacitor's voltage. The variation of modulation index as a function of capacitor voltage ripple is shown in Fig. 4.

This article has been accepted for publication in a future issue of this journal, but has not been fully edited. Content may change prior to final publication. Citation information: DOI 10.1109/TPEL.2018.2849104, IEEE Transactions on Power Electronics

Here the modulated signal is generated from a pure sinusoidal waveform by applying capacitor voltage ripple compensation [43].

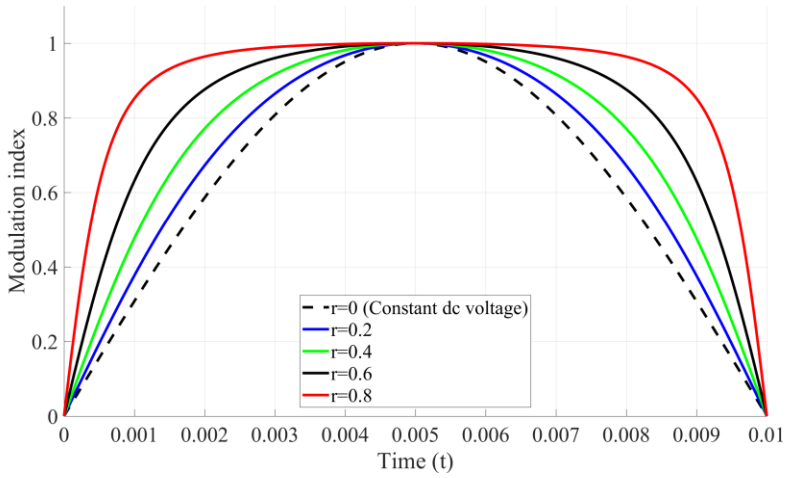

Fig. 4. Variation of the modulation index with the capacitor voltage ripple.

IV. MODULAR FILTER INDUCTOR

The voltage THD of LC-StatCom at the rated current, where the capacitor voltage ripple is largest, is lowest. Therefore, LC-StatCom will need a smaller inductor or lower switching frequency to satisfy its current quality target at its nominal load. However, when the current decreases, the beneficial effect of capacitor voltage ripple on quality of the output voltage reduces. This effect coupled with a smaller inductive filter (or lower switching frequency) pushes the current TDD higher, which may exceed the regulation limits. Consequently, the filter inductor needs to be designed for the worst case scenario of r=0, which means LC-StatCom cannot benefit from improved voltage quality to reduce the filter inductance. In this section a modular inductive filter concept is introduced to tackle this problem. The proposed solution essentially replaces a fixed-value filter inductor with modular thyristor switched reactors (TSR) [44], which are a well-developed technology as related to Static Var Compensator (SVC) applications. This forms a hybrid between LC-StatCom and SVC technologies. The proposed modular filter inductor is shown in Fig. 5. This configuration reduces the overall required energy storage capacity by m times compared to using a fixed inductance, L, as shown in the following,

This article has been accepted for publication in a future issue of this journal, but has not been fully edited. Content may change prior to final publication. Citation information: DOI 10.1109/TPEL.2018.2849104, IEEE Transactions on Power Electronics

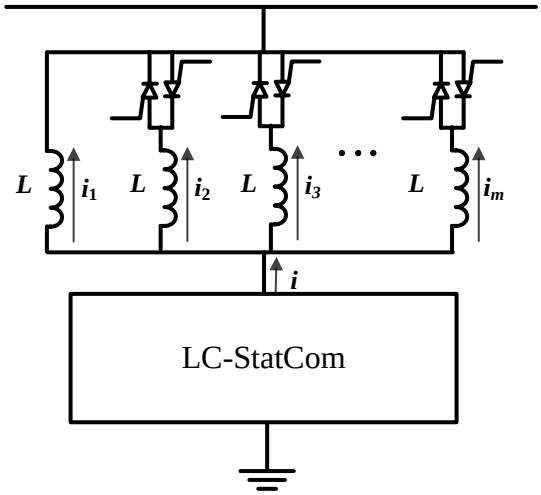

Fig. 5. The proposed modular inductive filter concept.

$$E = \frac{LI^2}{2m} \tag{14}$$

In (14), E is the stored magnetic energy in the inductor, m is the number of parallel connected submodules, and L represents the inductance.

The inductance of the proposed filter inductor, L_f, is a function of the current as given in (15). The inductance reduces as the current increases.

$$L_f = \begin{cases} \dfrac{mL_{f-n}}{\lceil mI_{g(p.u)} \rceil + 1} & , \quad I_{g(p.u)} < 1 \\ L_{f-n} & , \quad I_{g(p.u)} = 1 \end{cases} \tag{15}$$

$L_{f\text{-}n}$ is the inductance value at the rated condition ($I_{g(p.u)}$=1, $V_{(p.u)}$=1), which is equal to L/m. From (15), the voltage rating of the LC-StatCom with the proposed modular inductor is $1+X_{L(p.u)}/m$, which is reduced by (m-1) $X_{L(p.u)}/m$ compared to the fixed inductor case. Fig. 6 shows the effect of using the proposed modular inductor on the I-V characteristics of LC-StatCom.

This article has been accepted for publication in a future issue of this journal, but has not been fully edited. Content may change prior to final publication. Citation information: DOI 10.1109/TPEL.2018.2849104, IEEE Transactions on Power Electronics

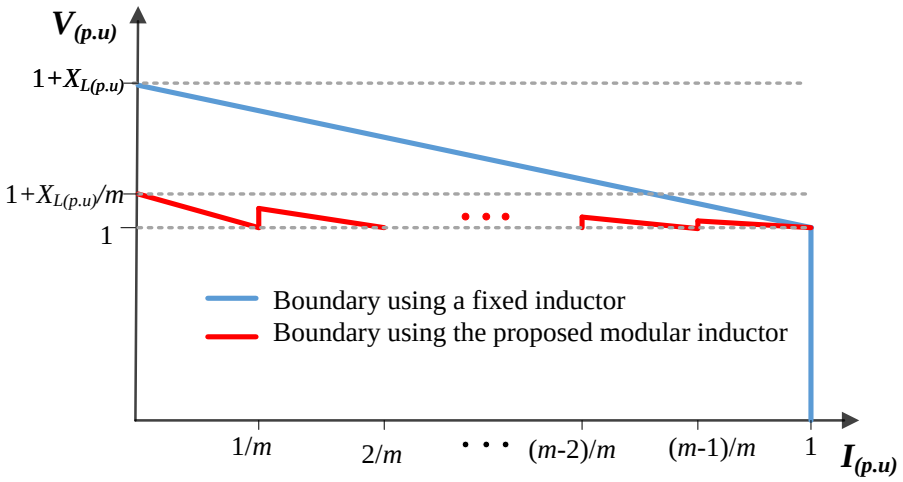

Fig. 6. LC-StatCom's I-V characteristic using fixed and the proposed modular filter inductor.

Utilization of naturally commutated switches, such as thyristors to switch inductors ensures the transition will happen at close to zero current where there is approximately zero energy stored in the magnetic field of the inductor, which would otherwise produce destructive over-voltages. Nevertheless, in high power applications a snubber circuit to control the voltage transients during thyristor turn off may be necessary [45], [46]. Thyristors are also relatively cheap, robust, and have very low conduction losses [44]. The current rating of these thyristors is *m* times lower than the rating of the semiconductors used within the LC-StatCom. The voltage rating is equal to the maximum voltage drop across the filtering inductor. Therefore, these switches have a fractional voltage and current rating compared to the converter.

The modular inductor solution will improve the current quality for light loads. Therefore, the modular filter inductor concept is also applicable to a conventional StatCom system. However, in this case the objective cannot be reducing the energy storage capacity of the inductor as the ripple on the capacitor voltages remains negligible and the synthesized ac voltage quality does not change with the current. Nevertheless, the StatCom can benefit from the modular inductor concept to improve current quality under low currents. As the current magnitude decreases, the current THD increases. This effect can be countered by increasing the inductance value as much as *m* times. Here, the overall energy storage capacity of the inductor and the voltage rating of the converter remains unchanged. The proposed modular inductor concept improves current quality by increasing the filter inductance to the maximum allowed value without violating the maximum allowed voltage drop on the filter inductor. The effect of using such modular inductor on the conventional StatCom's I-V characteristic is shown in Fig. 7.

This article has been accepted for publication in a future issue of this journal, but has not been fully edited. Content may change prior to final publication. Citation information: DOI 10.1109/TPEL.2018.2849104, IEEE Transactions on Power Electronics

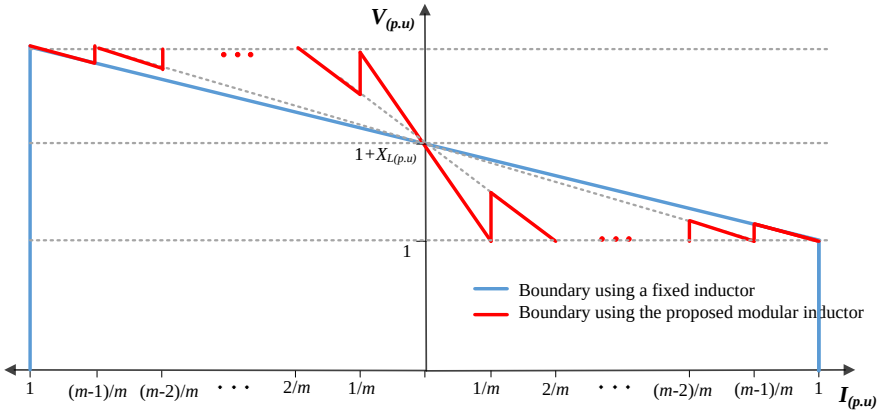

Fig. 7. Conventional StatCom's I-V characteristic using fixed and the proposed modular filter inductor.

V. MODULAR FILTER INDUCTOR DESIGN

The proposed modular filter inductor aims to compensate the adverse effect of increased PWM voltage THD on the ac current's TDD. From a theoretical point of view, a full compensation can only be achieved through use of a continuously variable L_f . The relation between the PWM voltage THD and weighted THD (WTHD), which is an indication for current TDD is depicted in Fig. 8. This figure is obtained using numerical calculations on a modulated waveform with the triangular carrier frequency 21 times higher than the reference waveform frequency. Effect of dc voltage ripple on the output current was eliminated using feedforward compensation on the reference waveform [43]. WTHD is defined as [47],

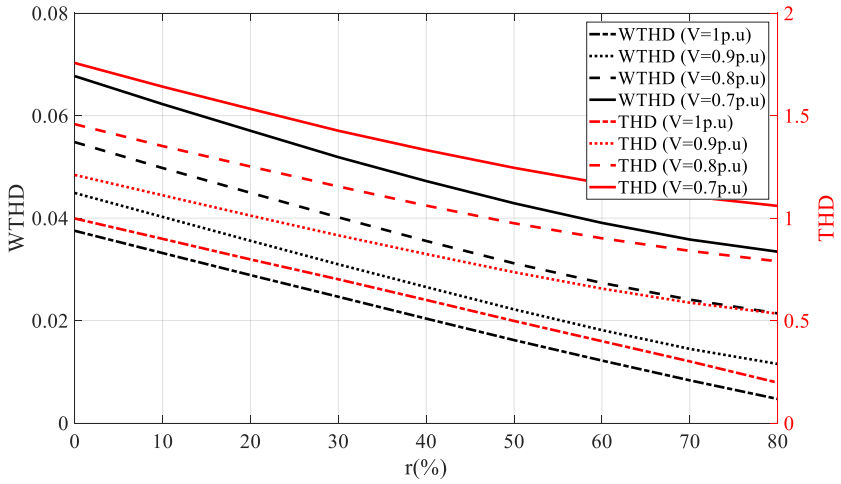

Fig. 8 Synthesized ac voltage THD and WTHD variation with ripple magnitude

This article has been accepted for publication in a future issue of this journal, but has not been fully edited. Content may change prior to final publication. Citation information: DOI 10.1109/TPEL.2018.2849104, IEEE Transactions on Power Electronics

$$WTHD = \frac{\sqrt{\sum_{n\neq 1}(V_{pwm}^2(n)/n^2)}}{V_{pwm}(1)}. \tag{16}$$

WTHD of v_{pwm} can be calculated numerically using the following equation [47].

$$WTHD = \sqrt{\frac{\int_0^{2\pi}(\int_0^{\theta} v_{pwm}(\theta)d\theta)^2 d\theta}{\pi V_{pwm}^2(1)} - 1} \tag{17}$$

where $\theta = 2\pi f_g t$.

Based on the results a linear relation between the current TDD and voltage THD is assumed, which is largely acceptable for the purpose of formulating L_f design. Current TDD also inversely relates to L_f.

$$TDD \propto \frac{THD}{L_f}. \tag{18}$$

Hence, in order to achieve a constant TDD, L_f needs to vary proportionally with the PWM voltage THD as follows,

$$L_f \propto THD. \tag{19}$$

PWM voltage THD for an ideal case where maximum ripple magnitude reaches 100% at nominal condition is derived in (9). In practice, however, maximum ripple, *R*, is usually lower than its theoretical 100% limit. A generalized form of (9) is

$$THD = \frac{\sqrt{2 - (1-(1-R)^2)I_{g(p.u)}V_{(p.u)} - V_{(p.u)}^2}}{V_{(p.u)}} \tag{20}$$

Fig. 9, show the variation of THD as a function of current for three different values of *R* and $V_{(p.u)}$. Each graph is normalized based on its own maximum value.

This article has been accepted for publication in a future issue of this journal, but has not been fully edited. Content may change prior to final publication. Citation information: DOI 10.1109/TPEL.2018.2849104, IEEE Transactions on Power Electronics

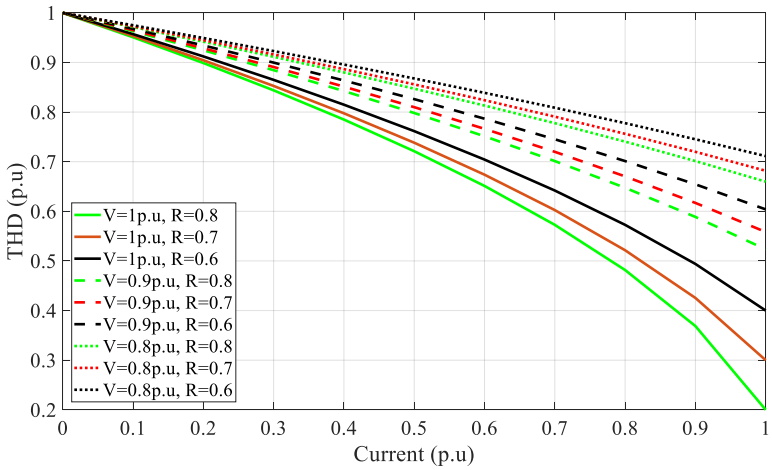

Fig. 9 Variation of THD as a function of current for different *V* and *R* values.

Although a continuously variable L_f, could be achievable using thyristor controlled reactor (TCR) technology, it is not attractive for filter inductor application as it adds large harmonics to the current. Therefore, discrete TSR units such as the one shown in Fig. 5 are employed. Although the choice of inductor value for each TSR branch can be different, identical TSR units are more favorable to maintain modularity of the system. Therefore, the current TDD variation can be estimated by replacing (15) and (20) in (18) as follows

$$TDD = \begin{matrix} \frac{TDD_n}{m}\left(\left[mI_{g(p.u)}\right]+1\right) & , & I_{g(p.u)} < 1 \\ TDD_n & , & I_{g(p.u)} = 1 \end{matrix} \tag{21}$$

Where,

$$TDD_n \propto \frac{\sqrt{2-(1-(1-R)^2)I_{g(p.u)}V_{(p.u)}-V_{(p.u)}^2}}{V_{(p.u)}L_{f-n}} \tag{22}$$

Selecting an appropriate value for the number of parallel connected inductor branches, *m*, is the next immediate question that needs to be answered to achieve the specified design objective. Here, the target is to keep TDD below

This article has been accepted for publication in a future issue of this journal, but has not been fully edited. Content may change prior to final publication. Citation information: DOI 10.1109/TPEL.2018.2849104, IEEE Transactions on Power Electronics

standard limits. In (22) R is a fixed parameter, but $V_{(p.u)}$ varies to some extent with current magnitude due to voltage drop across the filter inductor. However, this voltage variation is usually small and can be neglected. Therefore, for simplicity, the results in this section were obtained with the assumption of constant $V_{(p.u)}$. However, for better accuracy, this voltage variation can also be considered by calculating $V_{(p.u)}$ in (22) as follows,

$$V_{(p.u)} = \begin{cases} V_{g(p.u)}\left(1 + \dfrac{X_{f-n(p.u)} I_{g(p.u)} m}{\left[m I_{g(p.u)}\right] + 1}\right) & , \quad I_{g(p.u)} < 1 \\ V_{g(p.u)}\left(1 + X_{f-n(p.u)}\right) & , \quad I_{g(p.u)} = 1 \end{cases} \tag{23}$$

where, $X_{f\text{-}n}$ represents the reactance of $L_{f\text{-}n}$.

From (21), TDD at any given current is a function of m and $L_{f\text{-}n}$ (assuming a fixed switching frequency). TDD has, m, local maxima located at $I_{g(p.u)}/m$, $2I_{g(p.u)}/m$, …, and $I_{g(p.u)}$. In Fig. 10, the effect of adding more parallel branches for the case of V=0.9 p.u and R=0.6 is depicted. In this figure, $L_{f\text{-}n}$ remains constant. As expected, by increasing m overall TDD decreases. However, in practice only the maximum TDD, TDD_{max}, is the important parameter that needs to be below standard limits. For this case, the variation of TDD_{max} with m is shown in Fig. 11. Naturally, as m increases the TDD_{max} converges to TDD_n.

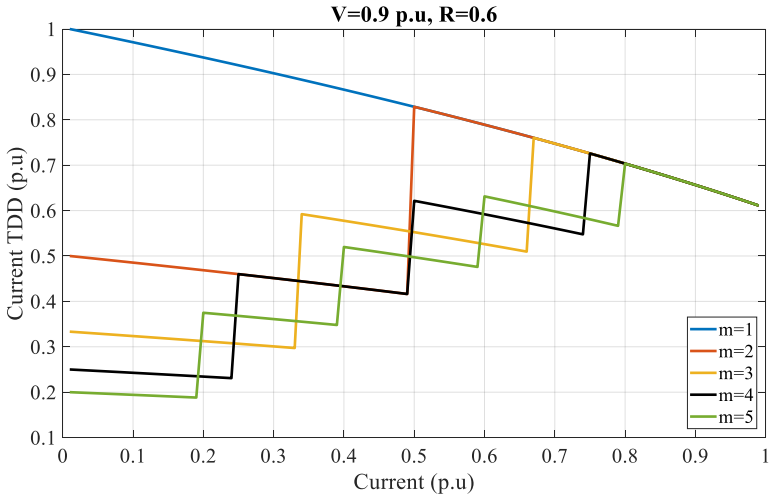

Fig. 10 Effect of increasing m on the current TDD profile

This article has been accepted for publication in a future issue of this journal, but has not been fully edited. Content may change prior to final publication. Citation information: DOI 10.1109/TPEL.2018.2849104, IEEE Transactions on Power Electronics

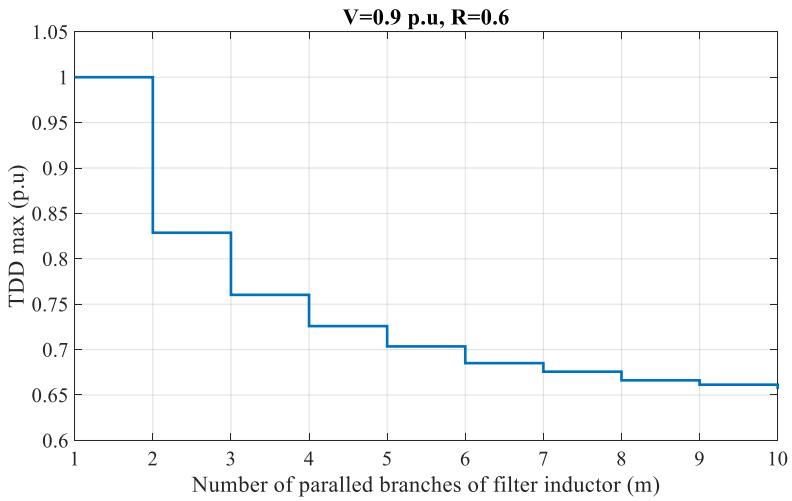

Fig. 11 Effect of increasing m on the TDD_{max}

The choice of $L_{f\text{-}n}$ and m must ensure that TDD remains below the standard limit at all of these local maxima. m has no effect on current quality at nominal condition. Therefore, TDD_n can only be regulated by $L_{f\text{-}n}$. Afterwards, TDD_{max} is controlled by m. A larger $L_{f\text{-}n}$, allows for using lower m value to meet the desired TDD_{max} target. However, by increasing $L_{f\text{-}n}$ the total size of magnetic components, the weight, and voltage rating of the converter increases. On the other hand, reducing $L_{f\text{-}n}$ will cause an increase in m, which adds to the complexity and potentially to the overall size of the system.

The results in this section highlight a key difference in designing an LC-StatCom compared to the conventional StatCom. In a StatCom system the sizing of inductance and switching frequency are performed to make sure the current TDD value at rated condition satisfies the standard requirement, whereas, in LC-StatCom such design parameters need to be determined at the location of maximum TDD, which occurs at a fraction of rated current.

In Table I, estimated $L_{f\text{-}n}$ for some practical values of $V_{(p.u)}$ and R are provided. For each case, $L_{f\text{-}n}$ is calculated using (21) to keep TDD_{max} fixed (equal to the maximum TDD of a system with m=1). $L_{f\text{-}n}$ then becomes a function of m in order to have a constant TDD_{max}. In this table, $L_{f\text{-}n}(m)$ is the required value of $L_{f\text{-}n}$ for an inductor with m number of parallel submodules. Therefore, in this table, $L_{f\text{-}n}(1)$ represents the inductance of a conventional fixed filter inductor to achieve a desired TDD_{max} limit. In practice, the achieved reduction in $L_{f\text{-}n}$ is expected to be lower due to the effect of other sources of harmonic pollution such as voltage imbalances and dead times. The estimation also does not take into account the effect of different modulators. Further, the assumption of a fixed value for $V_{(p.u)}$ is a source of minor error due to the voltage drop across the filter inductor, which depends on the current magnitude.

This article has been accepted for publication in a future issue of this journal, but has not been fully edited. Content may change prior to final publication. Citation information: DOI 10.1109/TPEL.2018.2849104, IEEE Transactions on Power Electronics

Hence, the provided data in this table is only for initial design reference and the final design objectives need to be verified through simulation.

TABLE I.

ESTIMATED $L_{F\text{-}N}$ VALUE USING MODULAR FILTER INDUCTOR CONCEPT COMPARED TO A SINGLE FILTER INDUCTOR SOLUTION

V(p.u)=0.8		
R	*m*	$L_{f\text{-}n}$(m)/ $L_{f\text{-}n}$(1)
0.5	2	0.88
	3	0.84
	4	0.82
0.6	2	0.87
	3	0.82
	4	0.8
0.7	2	0.86
	3	0.8
	4	0.78
V(p.u)=0.9		
0.5	2	0.85
	3	0.79
	4	0.76
0.6	2	0.83
	3	0.76
	4	0.73
0.7	2	0.81
	3	0.74
	4	0.7

VI. SIMULATIONS

Three-phase CHB converters are essentially three single-phase converters with a common neutral point. Therefore, without loss of generality, an eleven-level single-phase CHB StatCom is simulated in MATLAB/Simulink to determine the effectiveness of the proposed modular filter inductor. The parameters of this system are given in Table II [16]. The base 12 Ω impedance value to normalize $L_{f\text{-}n}$ is derived using nominal 6kV grid voltage and nominal 3MVA power rating of the converter.

TABLE II
PARAMETERS OF THE SIMULATED SYSTEM

Symbol	Quantity	Values
$V_{g\text{-}rms}$	Grid voltage *rms* value	6 kV
C	H-bridge DC capacitance	9.2×10^{-3} F
$L_{f\text{-}n}$	Filter inductance	3.5 mH (0.09 p.u)
$V_{c\text{-}ref}$	Capacitor reference voltage	1.9 kV
f_s	Switching frequency	500 Hz
f_g	Grid frequency	50 Hz
S	Converter nominal power	3 MVA
R_f	Filter inductor series resistance	0.2 Ω
f_v	Bandwidth of the voltage controller	10 Hz
f_i	Bandwidth of the current controller	100 Hz
N	Number of H-bridges	5

This article has been accepted for publication in a future issue of this journal, but has not been fully edited. Content may change prior to final publication. Citation information: DOI 10.1109/TPEL.2018.2849104, IEEE Transactions on Power Electronics

This StatCom design can be converted into LC-StatCom by adjusting the value of capacitance to target specific maximum ripple, *R* as follows,

$$C = \frac{2I_{gn}V_n}{N\omega R(2-R)V_{C-max}^2} \tag{24}$$

where the subscript *n* represents nominal parameters value. Selecting an optimal value for *R* is a complex optimization problem as it affects semiconductor ratings, capacitor size, efficiency, current quality, control design and dynamics of the system. Operation with larger values of *R* is favourable as it reduces the capacitor size and improves efficiency and current quality. However, voltage control challenges, current transient dynamics, and vulnerability to disturbances are among major limiting factors to increase *R*. In this section, a design based on, though not optimal, *R*=70% is selected for simulation.

Using 1900V as the maximum capacitor voltage, the capacitance of each H-bridge is 1.27 mF for reaching 70% maximum ripple. The overall diagram of the control system is shown in Fig. 12.

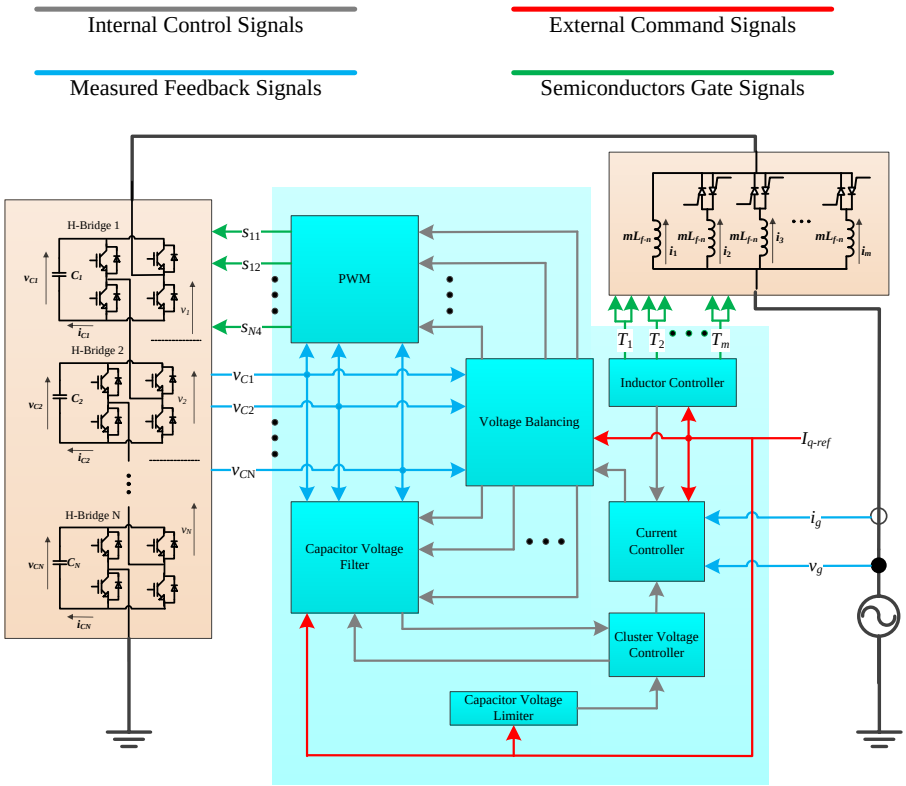

Fig. 12 Overview of LC-StatCom system with modular filter inductor

This article has been accepted for publication in a future issue of this journal, but has not been fully edited. Content may change prior to final publication. Citation information: DOI 10.1109/TPEL.2018.2849104, IEEE Transactions on Power Electronics

The modular inductor controller activates or deactivates inductor branches based on reference current magnitude. For a system with *m* number of parallel inductors, the *j*th unit activates if the current reference exceeds (*j*-1)/*m* p.u. Conversely, if the current goes below that threshold, the inductor goes offline. Both antiprallel thyristors share the same gate signal. When the gate signal is on, the switches start conducting (regardless of current magnitude or direction) to connect the parallel inductor. On the other hand, when the gate signal goes off, the conducting thyristor will remain conducting until the current goes below a certain value (ideally zero), after which the thyristor turns off. Operation around the threshold currents ((*j*-1)/*m* p.u, j=2, 3, …(*m*-1)) could cause rapid change of thryristor gate signals. This unwanted switching can easily be circumvented by introducing a hysteresis band in between the changeover of modes.

After each transition, the inductance value needs to be updated in the control system according to (15). The inductance affects mainly the operation of the voltage limiter and the current controller. The voltage limiter generates the reference signal, $V^2_{0\text{-}ref}$, for the cluster voltage controller to maintain a maximum 9500V total dc voltage (1900V per capacitor) using (3). Therefore, after each change in the filter inductor structure, X_L needs to be updated in this block. The disturbance caused by parameter adjustment in this block is insignificant as it only causes a minor correction in the generated reference signal. The effect of changing inductance on the current controller on the other hand is substantial and could cause large disturbances if not handled properly. Therefore, for the current controller, a predictive dead-beat current controller is utilized. The dead-beat controller calculates the ac voltage reference as follows [34],

$$v_{ref}^{k+1} = v_g^k + R_f i_g^k + L_f f_s \left(i_{g-ref}^{k+1} - i_g^k\right). \tag{25}$$

In (25), R_f is the resistance of filter inductor, subscript *ref* referes to reference signals, and superscripts *k* and *k+1* indicate the quantity values at present and future sampling instances, respectively. Updating the parameters in (25) is straightforward and the controller is able to respond to the filter inductor variation instantly and update the ac voltage reference for the next switching cycle.

The cluster voltage controller and voltage balancing blocks are implemented using simple proportional integral controllers [25]. The PWM block uses phase shifted PWM method to generate IGBT gate signals. Here, a feedforward compensation mechanism compensates the effect of large capcitor voltage ripples on the synthesized ac

This article has been accepted for publication in a future issue of this journal, but has not been fully edited. Content may change prior to final publication. Citation information: DOI 10.1109/TPEL.2018.2849104, IEEE Transactions on Power Electronics

voltage [47]. Finally, the capacitor voltage filtering block uses a feedforward filtering technique to prevent the capacitor voltage ripple from propagating through the control system [34].

In Fig. 13, the measured current TDDs and voltage THDs are depicted for both LC-StatCom and StatCom. The maximum ripple in this LC-StatCom design reaches 70%. Both systems have the same switching frequency and inductor value. Here, the target is to keep TDD below 2.5% . Allowing for some margin of error, TDD_{max} is limited to 2.4%. TDD_{max} for both LC-StatCom and StatCom are the same, which means both systems need to utilize similar filter inductors to satisfy TDD requirement. The difference is that in a conventional StatCom TDD remains constant independent of the current, whereas, LC-StatCom's TDD reduces for higher current. Therefore, LC-StatCom can benefit from modular filter structure to lower its TDD_{max}, which then allows for utilization of lower $L_{f\text{-}n}$ value (or lower switching frequency) to satisfy TDD requirements.

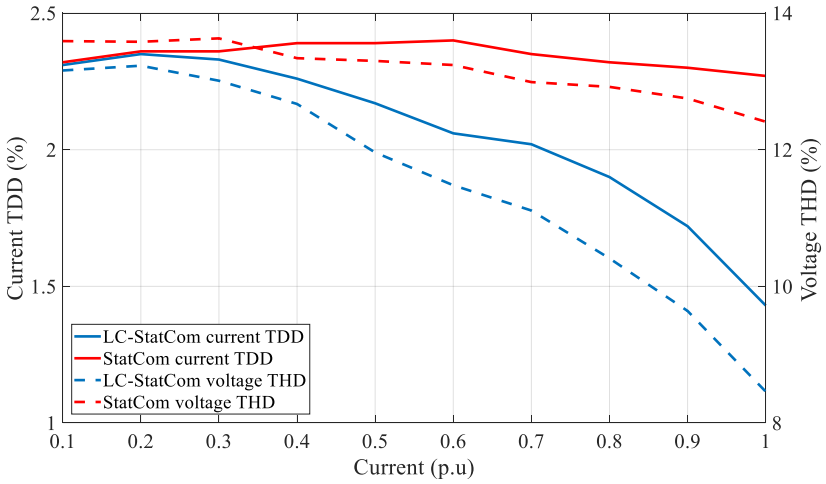

Fig. 13 Variation of current TDD and PWM ac voltage THD of StatCom and LC-StatCom systems

Based on the measured LC-StatCom's TDD profile, by using two parallel inductors $L_{f\text{-}n}$ needs to be approximately 3.16 mH to keep the TDD_{max} below 2.4 threshold at 0.5 p.u current local maxima. This value as expected is larger than theoretical 2.84 mH (derived from Table I for R=0.7 and $V_{p.u}$=0.9). The inductance of each inductor module is $2L_{f\text{-}n}$ which is 6.32 mH. Similarly by using three and four parallel inductor branches, $L_{f\text{-}n}$ is 2.97 mH and 2.84 mH, respectively (the theoretical value from Table I are 2.59 mH and 2.45 mH, respectively). The measured TDD profiles for each of these cases are shown in Fig. 14. As it can be seen the maximum TDD limit is satisfied in all of the cases.

This article has been accepted for publication in a future issue of this journal, but has not been fully edited. Content may change prior to final publication. Citation information: DOI 10.1109/TPEL.2018.2849104, IEEE Transactions on Power Electronics

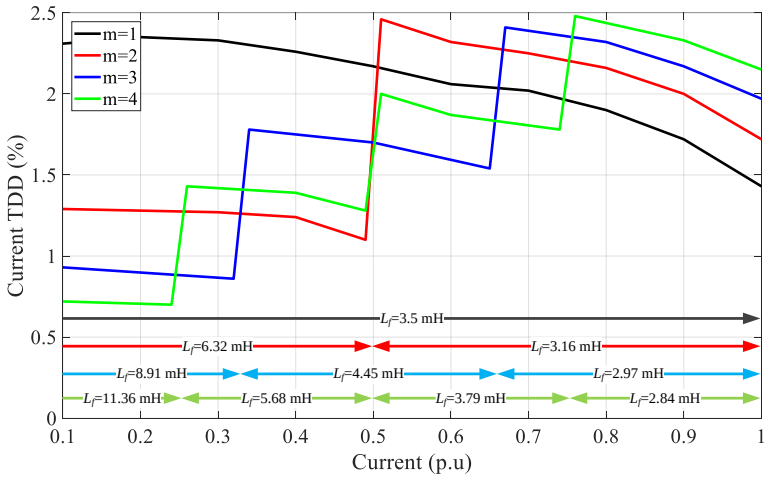

Fig. 14 Current TDD profile using modular inductive filter

VII. EXPERIMENTAL RESULTS

Operation of the LC-StatCom equipped with the proposed variable inductor is demonstrated by experiments on a 0.7-kVA seven-level single-phase system in which the filter inductor is composed by two submodules. Fig. 15 shows an overview of the LC-StatCom setup. The control system was implemented using dSPACE controller. The overall control architecture for the experiments was the same as the simulated circuit, which is shown in Fig. 12. The parameters of the experimental setup are given in Table III. The base 17.3 Ω impedance value to normalize $L_{f\text{-}n}$ is derived using nominal 110 V grid voltage and nominal 0.7 kVA power rating of the converter. The seven-level LC-StatCom was constructed by series connection of three POWEREX PP75B060 single-phase H-bridge converters. The system was connected to 240V grid voltage using an isolating step-down transformer to generate isolated 110V source voltage. Phase-shifted PWM was implemented using a DS5203 FPGA module. The PWM signals were transferred to the driver board by optical link for galvanic isolation. A DS2004 ADC module was used to send the feedback signals into the processor. All other control systems were implemented using a dSPACE DS1006 processor board.

This article has been accepted for publication in a future issue of this journal, but has not been fully edited. Content may change prior to final publication. Citation information: DOI 10.1109/TPEL.2018.2849104, IEEE Transactions on Power Electronics

TABLE III

PARAMETERS OF THE EXPERIMENTAL LC-STATCOM

Symbol	Quantity	Values
$V_{gn\text{-}rms}$	Grid voltage *rms* value	110 V (1 p.u)
C	Capacitance - H-bridge capacitors	520 μF
$L_{f\text{-}n}$	Filter inductor	5 mH (0.09 p.u)
f_s	Switching frequency (per H-bridge)	2 kHz
$V_{dc\text{-}max}$	Maximum voltage on capacitors	180 V
$V_{dc\text{-}min}$	Minimum voltage on capacitors	60 V
f_g	Grid frequency	50 Hz
S	Converter nominal power	700 VA
N	Number of H-bridges	3

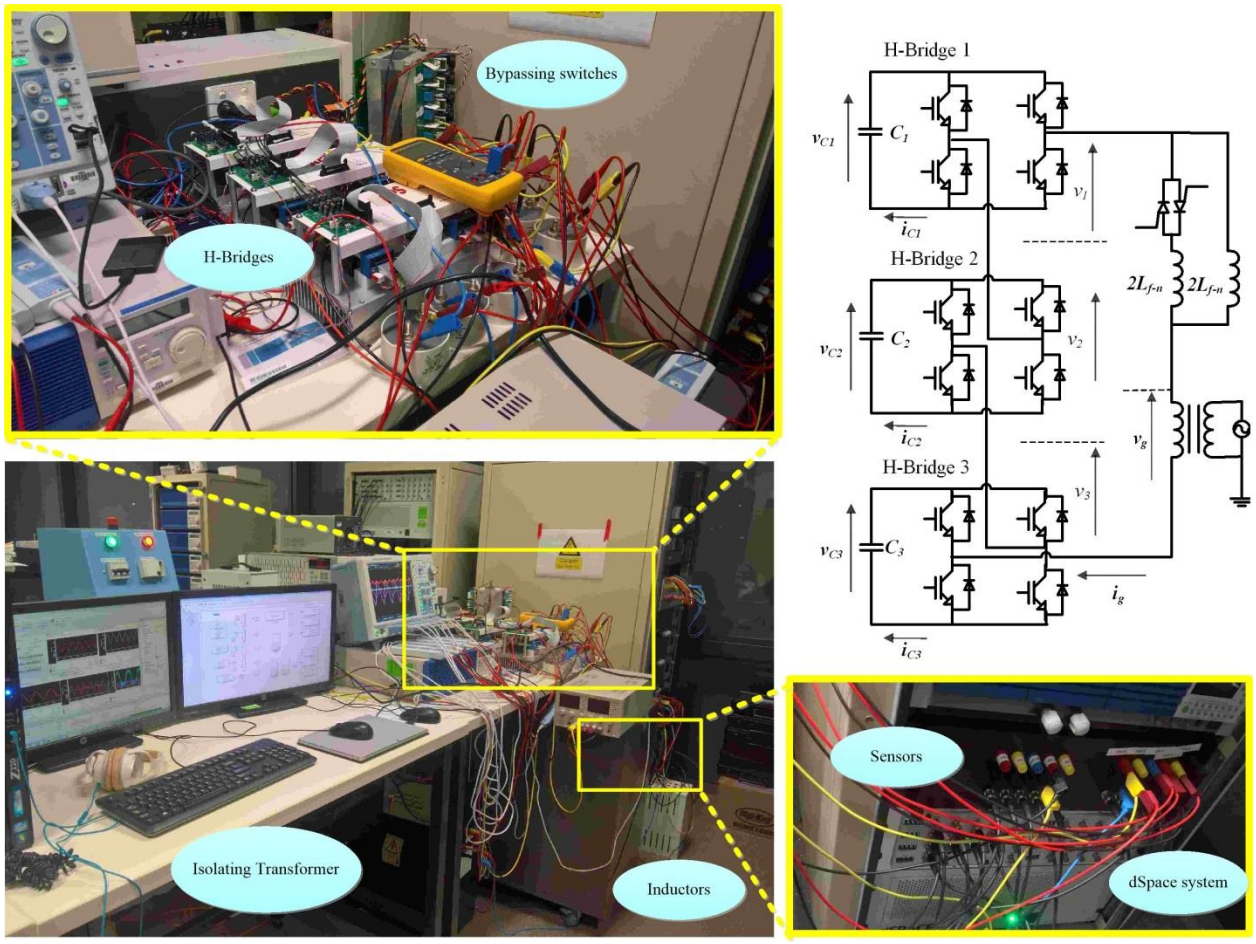

Fig. 15 Experimental setup.

This article has been accepted for publication in a future issue of this journal, but has not been fully edited. Content may change prior to final publication. Citation information: DOI 10.1109/TPEL.2018.2849104, IEEE Transactions on Power Electronics

Fig. 16 shows the voltage and current waveforms when the proposed LC-StatCom system is delivering its full load capacitive current. As can be seen, the LC-StatCom mainly operates on its highest (seventh) voltage level region, which highlights the LC-StatCom's excellent dc voltage utilization capability. As it can be seen, the grid current is equally divided between the two parallel inductive legs.

In this experimental setup, the threshold for disconnecting the parallel inductor is crossed when the current drops below 0.5 p.u. Fig. 17 shows the results for a case where the LC-StatCom is subjected to a step reactive current which involves switching the thyristors off. The LC-StatCom was initially supplying 0.8 p.u reactive current. At $t=t_0$ the reactive current reference abruptly changes to 0.4 p.u. As it can be seen the control system was able to quickly follow the reactive power command. In this case, the portion of the current passing through the parallel inductor continues to flow until the next zero crossing. It is important for the current controller to only adjust the control parameters after zero crossing to avoid any unwanted transients. The reverse case where the thyristors turn on following a step reactive current change from 0.4 p.u to 0.8 p.u at $t=t_0$ is shown in Fig. 18.

The significance of the proposed solution in improving the current quality is shown in Fig. 19. Here, the current THD for both fixed and modular inductor cases are recorded. The overall energy storage capacity of both inductors remains the same. As it can be seen for lower currents when the inductor value doubles, the THD becomes almost half. Further reduction of THD in lower currents can be achieved by utilizing more inductor submodules. However, the tradeoff is increased hardware and control complexity.

Improved current quality for low current can be easily seen from captured current waveforms in Fig. 20. In this figure, the dominant harmonics around first carrier frequency (6 kHz) are shown. Here, the third order harmonics and any other harmonic lower than 0.005 A are removed. Using this data, the TDD of the current for both cases are measured in Fig. 19. Based on the results, the maximum TDD of 1.5% for a fixed inductor case appears at low current where the ripple is negligible. For the modular inductor with the same size, TDD reaches its peak of 1.3% at 0.5 p.u current immediately after the parallel inductor is switched on. Therefore, in order to reach a comparable maximum TDD of 1.5%, the modular inductor's energy storage capacity can be about 13% smaller.

This article has been accepted for publication in a future issue of this journal, but has not been fully edited. Content may change prior to final publication. Citation information: DOI 10.1109/TPEL.2018.2849104, IEEE Transactions on Power Electronics

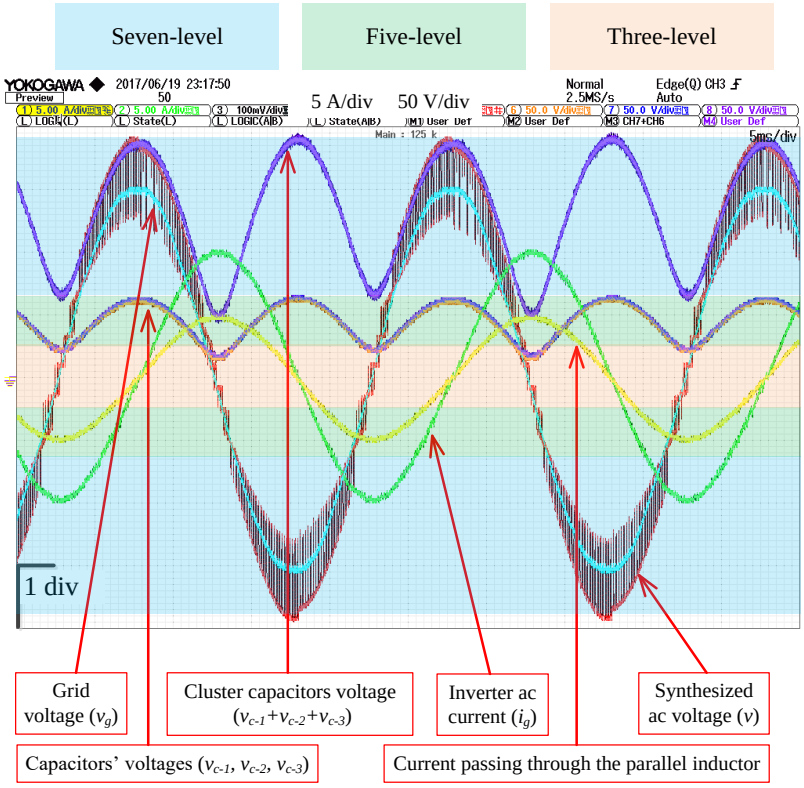

Fig. 16 Operation of the modular inductor equipped LC-StatCom delivering its rated capacitive current.

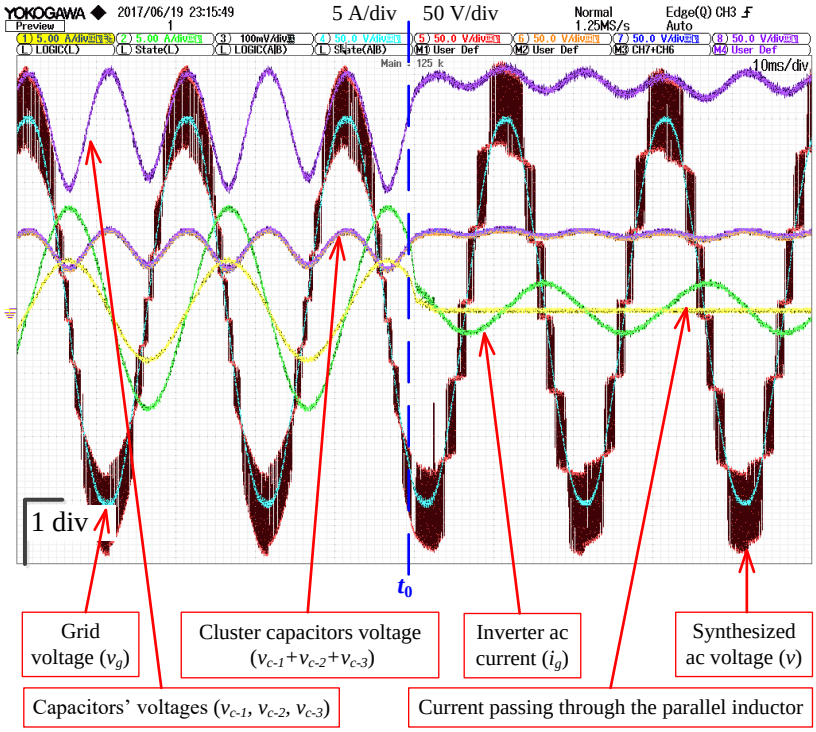

Fig. 17 Performance of the modular inductor equipped LC-StatCom during step reactive current change from 0.8 p.u to 0.4 p.u at t_0.

This article has been accepted for publication in a future issue of this journal, but has not been fully edited. Content may change prior to final publication. Citation information: DOI 10.1109/TPEL.2018.2849104, IEEE Transactions on Power Electronics

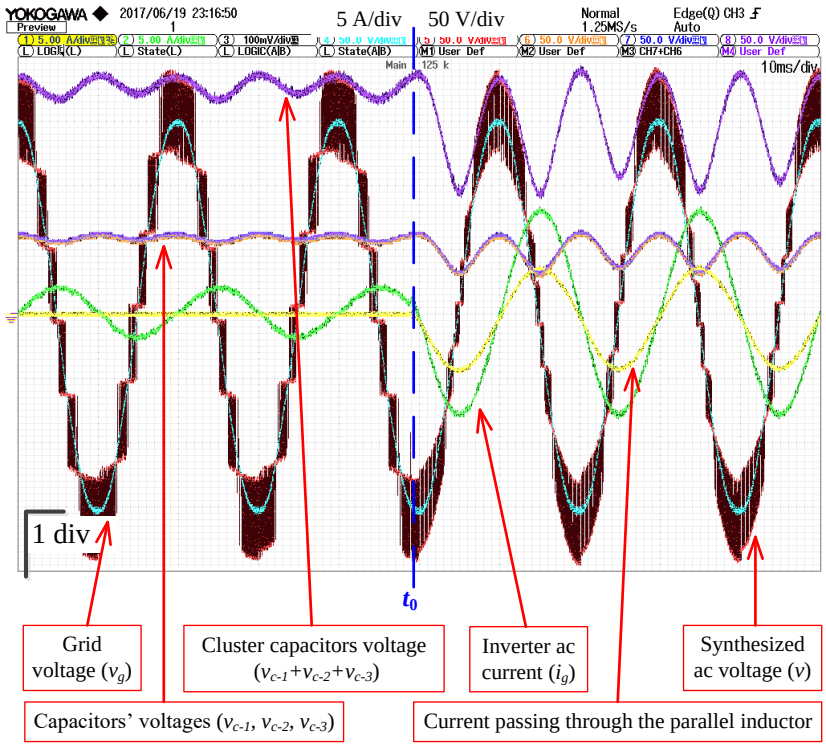

Fig. 18 Performance of the modular inductor equipped LC-StatCom during step reactive current change from 0.4 p.u to 0.8 p.u at t_0.

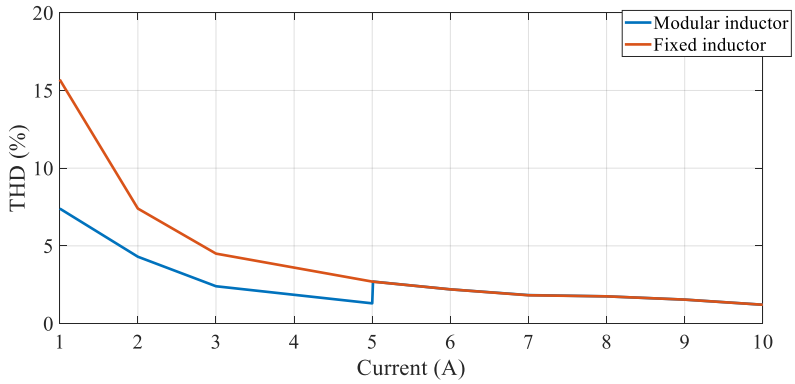

Fig. 19 Comparison of current THD between LC-StatCom with fixed filter inductor and with the proposed modular inductor.

This article has been accepted for publication in a future issue of this journal, but has not been fully edited. Content may change prior to final publication. Citation information: DOI 10.1109/TPEL.2018.2849104, IEEE Transactions on Power Electronics

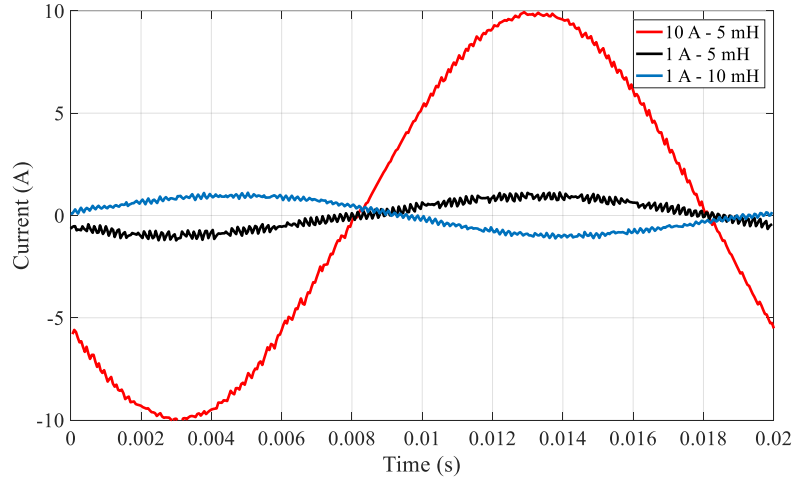

(a)

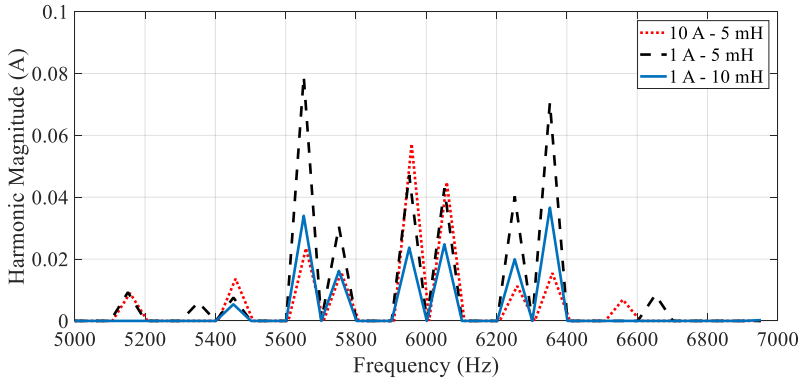

(b)

Fig. 20 (a) Experimental current waveforms and (b) their corresponding dominant harmonics.

This article has been accepted for publication in a future issue of this journal, but has not been fully edited. Content may change prior to final publication. Citation information: DOI 10.1109/TPEL.2018.2849104, IEEE Transactions on Power Electronics

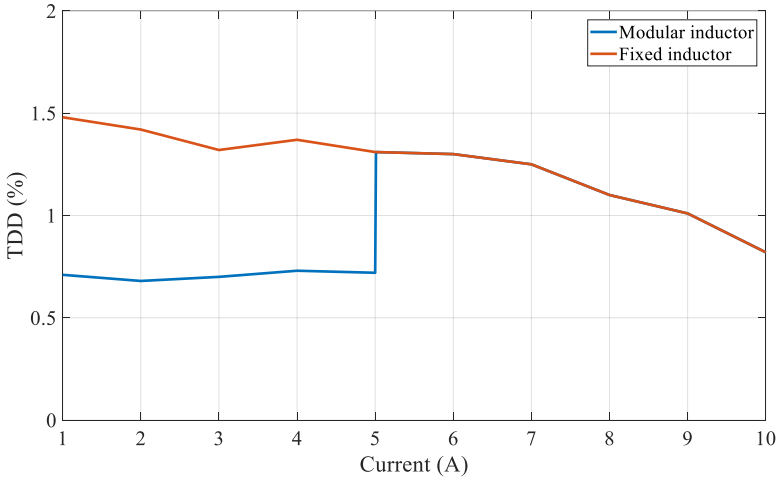

Fig. 14. Experimental results to compare the current TDD between the LC-StatCom with fixed filter inductor and with the proposed modular inductor.

VIII. CONCLUSION

A modular filter inductor concept for LC-StatCom has been suggested to further reduce the energy storage capacity of the filter inductor. Lower inductance reduces the voltage rating of the converter. The feasibility of the proposed system is verified through experiments on a small scale CHB LC-StatCom prototype. The developed experimental setup was equipped with a modular inductor with two parallel legs. Therefore, the filter inductance size, for currents lower than 0.5 p.u is doubled, which caused a reduction in the current THD by almost 50%. The prediction based on current TDD behaviour suggests up to 13% reduction in filter inductor's energy storage capacity using the proposed modular inductor. A detailed analysis on designing the modular inductor in order to determine its real volume, weight, and cost is one of the main remaining issues, which has not been covered in this manuscript.

IX. ACKNOWLEDGMENT

This work was supported by the Singapore Ministry of Education Academic Research Fund Tier 1.

X. REFERENCES

[1] Y. Neyshabouri, H. Iman-Eini, and M. Miranbeigi, "State feedback control strategy and voltage balancing scheme for a transformer-less STATic synchronous COMpensator based on cascaded H-bridge converter," *IET Power Electron.*, vol. 8, pp. 906-917, Jun. 2015.

[2] L. K. Haw, M. S. A. Dahidah, and H. A. F. Almurib, "A new reactive current reference algorithm for the STATCOM system based on cascaded multilevel inverters," *IEEE Trans. Power Electron.*, vol. 30, pp. 3577-3588, Jul. 2015.

[3] H. Law Kah, M. S. A. Dahidah, and H. A. F. Almurib, "SHE PWM cascaded multilevel inverter with adjustable DC voltage levels control for STATCOM applications," *IEEE Trans. Power Electron.*, vol. 29, pp. 6433-6444, Dec. 2014.

[4] C. D. Townsend, T. J. Summers, and R. E. Betz, "Impact of practical issues on the harmonic performance of phase-shifted modulation strategies for a cascaded H-bridge StatCom," *IEEE Trans. Ind. Electron.*, vol. 61, pp. 2655-2664, Jun. 2014.

[5] C. t. Lee, B. s. Wang, S. w. Chen, S. f. Chou, J. l. Huang, P. t. Cheng, H. Akagi, and P. Barbosa, "Average power balancing control of a STATCOM based on the cascaded H-bridge PWM converter with star configuration," *IEEE Trans. Ind. Appl.*, vol. 50, pp. 3893-3901, Nov. -Dec. 2014.

[6] R. Xu, Y. Yu, R. Yang, G. Wang, D. Xu, B. Li, and S. Sui, "A novel control method for transformerless H-bridge cascaded STATCOM with star configuration," *IEEE Trans. Power Electron.*, vol. 30, pp. 1189-1202, Mar. 2015.

[7] H. Akagi, S. Inoue, and T. Yoshii, "Control and performance of a transformerless cascade PWM STATCOM with star configuration," *IEEE Trans. Ind. Appl.*, vol. 43, pp. 1041-1049, Jul. -Aug. 2007.

[8] Y. Li and B. Wu, "A novel DC voltage detection technique in the CHB inverter-based STATCOM," *IEEE Trans. Power Del.*, vol. 23, pp. 1613-1619, Jul. 2008.

[9] J. A. Barrena, L. Marroyo, M, V. Rodriguez, and J. R. T. Apraiz, "Individual voltage balancing strategy for PWM cascaded H-bridge converter-based STATCOM," *IEEE Trans. Ind. Electron.*, vol. 55, pp. 21-29, Jan. 2008.

[10] C. Han, A. Q. Huang, Y. Liu, and B. Chen, "A generalized control strategy of per-phase DC voltage balancing for cascaded multilevel converter-based STATCOM," in *Proc. IEEE PESC*, pp. 1746-1752, 2007.

[11] W. Song and A. Q. Huang, "Fault-tolerant design and control strategy for cascaded H-bridge multilevel converter-based STATCOM," *IEEE Trans. Ind. Electron.*, vol. 57, pp. 2700-2708, Aug. 2010.

[12] Y. Liu, A. Q. Huang, W. Song, S. Bhattacharya, and G. Tan, "Small-signal model-based control strategy for balancing individual DC capacitor voltages in cascade multilevel inverter-based STATCOM," *IEEE Trans. Ind. Electron.*, vol. 56, pp. 2259-2269, Jun. 2009.

[13] N. Hatano and T. Ise, "Control scheme of cascaded H-bridge STATCOM using zero-sequence voltage and negative-sequence current," *IEEE Trans. Power Del.*, vol. 25, pp. 543-550, Apr. 2010.

[14] C. D. Townsend, T. J. Summers, J. Vodden, A. J. Watson, R. E. Betz, and J. C. Clare, "Optimization of switching losses and capacitor voltage ripple using model predictive control of a cascaded H-bridge multilevel StatCom," *IEEE Trans. Power Electron.*, vol. 28, pp. 3077-3087, Jul. 2013.

[15] C. D. Townsend, T. J. Summers, and R. E. Betz, "Multigoal heuristic model predictive control technique applied to a cascaded H-bridge StatCom," *IEEE Trans. Power Electron.*, vol. 27, pp. 1191-1200, Mar. 2012.

[16] B. Gultekin and M. Ermis, "Cascaded multilevel converter-based transmission STATCOM: system design methodology and development of a 12 kV ±12 MVAr power stage," *IEEE Trans. Power Electron.*, vol. 28, pp. 4930-4950, Nov. 2013.

[17] G. Farivar, B. Hredzak, and V. G. Agelidis, "Reduced-capacitance thin-film H-bridge multilevel STATCOM control utilizing an analytic fltering scheme," *IEEE Trans. Ind. Electron.*, vol. 62, pp. 6457-6468, Oct. 2015.

[18] G. Farivar, V. G. Agelidis, and B. Hredzak, "A generalized capacitors voltage estimation scheme for multilevel converters," in *Proc EPE'14-ECCE*, pp. 1-5, 2014.

[19] B. Gültekin, "Cascaded multilevel converter based transmission StatCom: system design methodology and development of a 12kv ±12 MVAR powerstage," PhD. dissertation, Dept. Elect. Eng., Middle East Technical Univ., Ankara, Turkey, 2012.

[20] Y. Neyshabouri and H. Iman-Eini, "A New Fault Tolerant Strategy for a Cascaded H-Bridge Based STATCOM," *IEEE Trans. Ind. Electron.* vol. 65, no. 8, pp. 6436-6445, Aug. 2018.

[21] E. Behrouzian and M. Bongiorno, "Investigation of Negative-Sequence Injection Capability of Cascaded H-Bridge Converters in Star and Delta Configuration," *IEEE Trans. Power Electron.*, vol. 32, no. 2, pp. 1675-1683, Feb. 2017.

[22] P. H. Wu, H. C. Chen, Y. T. Chang and P. T. Cheng, "Delta-Connected Cascaded H-Bridge Converter Application in Unbalanced Load Compensation," *IEEE Trans. Ind. Appl.*, vol. 53, no. 2, pp. 1254-1262, March-April 2017.

[23] J. J. Jung, J. H. Lee, S. K. Sul, G. T. Son and Y. H. Chung, "DC Capacitor Voltage Balancing Control for Delta-Connected Cascaded H-Bridge STATCOM Considering Unbalanced Grid and Load Conditions," *IEEE Trans. Power Electron.*, (Early Access).

[24] H. C. Chen and P. T. Cheng, "A DC Bus Voltage Balancing Technique for the Cascaded H-Bridge STATCOM With Improved Reliability Under Grid Faults," *IEEE Trans. Ind. Appl.*, vol. 53, no. 2, pp. 1263-1270, March-April 2017.

[25] G. Farivar, B. Hredzak, and V. G. Agelidis, "Decoupled control system for cascaded H-bridge multilevel converter based STATCOM," *IEEE Trans. Ind. Electron.*, vol. 63, pp. 322-331, Jan. 2016.

[26] D. Lu, J. Zhu, J. Wang, J. Yao, S. Wang and H. Hu, "Simple Zero-Sequence-Voltage-Based Cluster Voltage Balancing Control and the Negative Sequence Current Compensation Regulation Identification for Star-Connected Cascaded H-Bridge STATCOM," *IEEE Trans. Power Electron.*, (Early Access).

[27] D. Lu *et al*., "Clustered Voltage Balancing Mechanism and Its Control Strategy for Star-Connected Cascaded H-Bridge STATCOM," *IEEE Trans. Ind. Electron.*, vol. 64, no. 10, pp. 7623-7633, Oct. 2017

[28] Y. Zhang, X. Wu and X. Yuan, "A Simplified Branch and Bound Approach for Model Predictive Control of Multilevel Cascaded H-Bridge STATCOM," *IEEE Trans. Ind. Electron.*, vol. 64, no. 10, pp. 7634-7644, Oct. 2017.

[29] I. Jahn, C. D. Townsend and H. Z. de la Parra, "Model-predictive modulation strategy for a hybrid Si-SiC cascaded H-bridge multi-level converter," in *Proc.EPE'16 ECCE Europe*, Karlsruhe, 2016, pp. 1-10.

[30] Y. Zhang, X. Wu, X. Yuan, Y. Wang and P. Dai, "Fast Model Predictive Control for Multilevel Cascaded H-Bridge STATCOM With Polynomial Computation Time," *IEEE Trans. Ind. Electron.*, vol. 63, no. 8, pp. 5231-5243, Aug. 2016.

[31] T. Hussain and A. Das, "Dodecagonal space vector PWM for cascaded H-bridge based STATCOM," in *Proc. IEEE UPCON*, Mathura, 2017, pp. 150-155.

[32] E. Behrouzian, M. Bongiorno and R. Teodorescu, "Impact of Switching Harmonics on Capacitor Cells Balancing in Phase-Shifted PWM-Based Cascaded H-Bridge STATCOM," *IEEE Trans. Power Electron.*, vol. 32, no. 1, pp. 815-824, Jan. 2017.

[33] H. Geng, S. Li, C. Zhang, G. Yang, L. Dong and B. Nahid-Mobarakeh, "Hybrid Communication Topology and Protocol for Distributed-Controlled Cascaded H-Bridge Multilevel STATCOM," *IEEE Trans. Ind. Appl.*, vol. 53, no. 1, pp. 576-584, Jan.-Feb. 2017.

[34] G. Farivar, C. Townsend, B. Hredzak, J. Pou, and V. Agelidis, "A low capacitance cascaded H-bridge multi-level StatCom," *IEEE Trans. Power Electron.*, vol. 32, no. 3, pp. 1744-1754, Mar. 2017.

[35] G. Farivar, J. Pou and A. Tripathi, "LC-StatCom with symmetrical I-V characteristic: Total Harmonic Distortion Study," in *Proc. ACEPT*, Singapore, 2017, pp. 1-5.

[36] T. Isobe, D. Shiojima, K. Kato, Y. R. R. Hernandez and R. Shimada, "Full-bridge reactive power compensator with minimized-equipped capacitor and its application to static VAR compensator," *IEEE Trans. Power Electron.*, vol. 31, no. 1, pp. 224-234, Jan. 2016.

[37] Zijin He, L. Zhang, T. Isobe and H. Tadano, "Dynamic performance improvement of single-phase STATCOM with drastically reduced capacitance", in *Proc. IFEEC-ECCE Asia*, pp. 1413-1418, 2017.

[38] T. Isobe, L. Zhang, H. Tadano, J. A. Suul and M. Molinas, "Control of DC-capacitor peak voltage in reduced capacitance single-phase STATCOM", in *Proc. IEEE COMPEL*, pp. 1-8, 2016.

[39] G. Farivar, C. D. Townsend, B. Hredzak, J. Pou and V. G. Agelidis, "Passive reactor compensated cascaded H-bridge multilevel LC-StatCom," *IEEE Trans. Power Electron.*, vol. 32, no. 11, pp. 8338-8348, Nov. 2017.

[40] G. Farivar and J. Pou, "LC-StatCom with symmetrical I-V characteristic — Power loss analysis," in *Proc. EPE'17 ECCE Europe*, Warsaw, 2017, pp. P.1-P.10.

[41] B. Karanayil, V.G. Agelidis, and J. Pou, "Evaluation of dc-link decoupling using electrolytic or polypropylene film capacitors in three-phase grid-connected photovoltaic inverters," in *Proc. IEEE IECON*, pp. 6980-6986, 10-13, Nov. 2013.

[42] H. Wang and F. Blaabjerg, "Reliability of capacitors for dc-link applications in power electronic converters – An overview", *IEEE Trans. Ind. Appl.*, vol. 50, no. 5, pp. 3569-3578, Sep.-Oct. 2014.

[43] S. Kouro; P. Lezana; M. Angulo; J. Rodriguez, "Multicarrier PWM With DC-Link Ripple Feedforward Compensation for Multilevel Inverters," *IEEE Trans. Power Electron.*, vol.23, no.1, pp.52-59, Jan. 2008

[44] Narain G. Hingorani and Laszlo Gyugyi, "Power semiconductor devices," in *Understanding FACTS: Concepts and Technology of Flexible AC Transmission Systems*, 1, Wiley-IEEE Press, pp.37-66, 2000.

[45] Chang Woo Lee and Song Bai Park, "Design of a thyristor snubber circuit by considering the reverse recovery process," *IEEE Trans. Power Electron.*, vol. 3, no. 4, pp. 440-446, Oct. 1988.

[46] M. O. Popescu, D. Nistor, and C. Popescu, "R-C snubber for thyristor turn-off-a new approach," in *Proc. IEEE International Symposium on Industrial Electronics (ISIE)*, Warsaw, vol. 1, pp. 505-507, 1996.

[47] D. Grahame Holmes; Thomas A. Lipo, "Harmonic Distortion," in *Pulse Width Modulation for Power Converters: Principles and Practice* , 1, Wiley-IEEE Press, 2003, pp.744-